

# Laser Bending of Tubes: Mechanism, Analysis, and Prediction

Wenchuan Li

Y. Lawrence Yao

Department of Mechanical Engineering,  
Columbia University,  
New York, NY 10027

*Laser bending of tubes is a process in which laser-induced thermal distortion is used to bend tubes without hard tooling or external forces. Mechanisms of the process are examined to better understand the deformation characteristics such as wall thickness variation, cross-section ovalization, bending radius, and asymmetry. Factors important to these characteristics are experimentally and numerically investigated. Temporal and spatial distributions of temperature and stress/strain obtained from experimentally validated simulation models are also used to better understand additional phenomena accompanying the process, and to help devise ways to improve the process such as reducing asymmetry. A closed-form expression for the bending angle is proposed.*

[DOI: 10.1115/1.1392992]

## 1 Introduction

Tube bending is important in the manufacturing of boilers, engines, heat exchangers, air conditioners, and tubing and pipe products. Tubes may be mechanically bent either when hot or cold, although most bending is done cold. Cold bending is more efficient and yields more rigid products, while hot bending is suitable for bends of smaller bending radii or tubes of larger diameter.

During the bending of a tube, the material at the extrados (the free outer surface, while the intrados is the inner surface contacting the die) generally becomes thinner when it is subjected to tensile stress. This may induce a neck formation or fracture so that tensile failure occurs. To prevent thinning, pressure bending may be used. This makes the production facilities more complicated. Buckling or wrinkling of the material at the intrados may occur due to compressive stress during the bending. The buckling becomes more acute for thin sections. To prevent undesirable forming defects such as buckling and distortion of the ring cross section, mandrels can be used.

There is a minimum bending radius to which a tube can be bent in the mechanical bending. This is mainly because of the possibilities of the tensile failure in the extrados as mentioned above. The minimum radius is proportional to the outer diameter of the tube and inversely proportional to the percent elongation of material [1]. Tubes that are to be bent to small radii frequently have to be annealed to increase their ductility, which increases the complexity of the bending process.

The bending of tubes may be accompanied by flattening of the tube cross section. This is because the material at the extrados tends to move inward in response to the tensile stress caused by external bending moment, and compressive forces are applied at the intrados from the bending die. The flattening of elastic tubes under the bending was first analyzed by Von Karman [2]. Brazier [3] extended the analysis to include nonlinear effects. It has been called the *Brazier effect*. An approximate displacement field and the strain energy and its Euler equation were proposed. Wall thickness change could not be included in the analysis. Zhang and Yu [4] investigated the Brazier effect of infinitely long cylindrical tubes under elastic-plastic bending by the energy method and obtained the expressions for bending moment and flattening ratio in terms of curvature. The Brazier effect in cylindrical tubes under pure plastic bending was studied [5]. The degree of ovalization was determined using a postulate of a minimum instantaneous

bending moment. Pan and Stelson [6] investigated the relationships between the axial curvature of a bent tube and the resulting cross-section deformation for a finite-length tube by an analytic approach. An approximate expression obtained for the displacement field described ovalization, wall thickness variation in addition to the others, which were in agreement with experimental measurements.

## 2 Laser Bending of Tubes

Laser bending of tubes has the following advantages over mechanical bending of tubes. Neither a hard bending tool nor external forces are required, and thus the cost of tube bending is greatly reduced for small-batch production and prototyping. Wall thickness reduction seems to be avoided and lesser ovalization results. With the flexibility of the laser beam delivery and numerical control systems, it is easier to automate the process. Tube laser bending has the potential to deal with materials whose bending normally requires repeated annealing when conventional mechanical means are used.

Silve et al., [7] investigated procedures for laser bending of square cross-section tubes of mild steel. Different scanning sequences were compared experimentally. Bending angles and profiles, variation in thickness, and plastic compression were also studied. Laser shaping of tubes and the microstructure of formed parts was investigated [8], but no details were given. Kraus [9] conducted an FEM study of laser bending of square cross-section tubes and studied the temporal development of plastic straining and restraining in the bending process. It was found that although the process is dominated by the upsetting mechanism, an inhomogeneous plastic zone exists at the beginning of the scanning. In the cooling-off phase after the scanning, a plastic restraining may take place, which depends on the strain, the cross-section geometry, and properties of the material scanned. The sequence of heating was also investigated by the simulation but no experimental validation was conducted.

In the present work, the mechanism of tube laser bending is studied in more detail through numerical and experimental investigations. The causes for various aspects of deformation characteristics such as wall thickness variation, ovalization, protruded intrados, and bending radius are explained. Other characteristics of laser bent tubes such as asymmetry of deformation and the ways to reduce asymmetry, are also examined.

## 3 Mechanism of Laser Bending of Tubes

It is generally known that laser bending of tubes is achieved through the upsetting mechanism. Consider the circular tube

Contributed by the Manufacturing Engineering Division for publication in the JOURNAL OF MANUFACTURING SCIENCE AND ENGINEERING. Manuscript received Aug. 2000; revised Feb. 2001. Associate Editor: S. Kapoor.

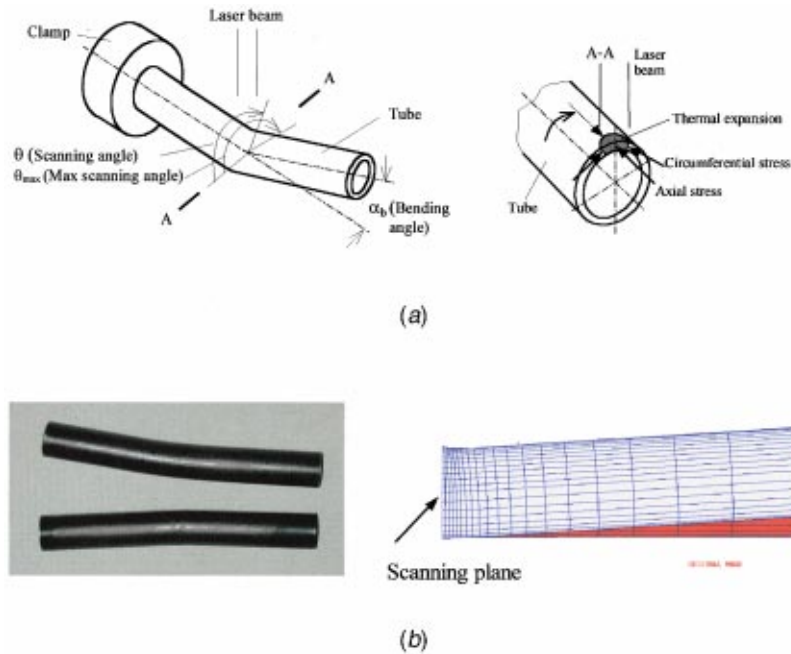


**Fig. 1** (a) Schematic of laser bending of tubes (left) and direction of thermal—induced stresses in the cross section A-A (right) (b) Samples of laser bent tubes (outer diameter 12.7 mm and thickness 0.89 mm) and simulation result of laser bent tube (half tube shown due to symmetry about the scanning plane, deformation magnification  $\times 5$ , note the protruded intrados near the symmetry plane, power: 780 W, angular speed: 1.57 rad/s, beam diameter: 11 mm, maximum scanning angle,  $\theta_{max}$ : 180 degree, tube outer diameter: 12.7 mm, wall thickness: 0.89 mm)

shown in Fig. 1. The tube rotates typically 180 degrees or more when its outer circumference is heated by a laser beam. The laser beam size is so chosen to be much greater than the tube thickness. As a result, the scanned region of the tube is heated almost homogeneously in the thickness direction, and undergoes compressive plastic deformation and wall thickening due to restriction on thermal expansion by the surrounding material. The shortening in the scanned region (in the axial direction of the tube) subsequently causes the tube to bend towards the laser beam.

A more detailed examination of the upsetting mechanism may help better understand the bending process. The thermally induced compressive stresses are exerted on the heat-affected region in both the axial and circumferential directions as shown in Fig. 1(a). The axial stress is more significant and is primarily responsible for the wall thickening, while the vertical component of the circumferential stress tends to make material in the area move outward. Therefore, the deformation in the region is a combination of the shortening along the axial direction of the tube and the displacement outward in the radial direction.

Since laser bending of tubes is mainly made possible by the axial plastic shortening at the intrados via the above-mentioned mechanism, the tensile deformation at the extrados is much less than that in mechanical bending. By properly adjusting process parameters, the wall thinning at the extrados can be greatly reduced or nearly avoided.

For the same reason, the minimum bending radius is not determined by the tensile failure at the extrados in laser forming of tubes. This means the elongation of the material and the outer diameter may no longer be the main factors affecting the minimum bending radius as mentioned earlier for mechanical bending. Other parameters such as laser beam diameter may play a more important role in determining the minimum bending radius.

In mechanical bending, ovalization is caused by the external force exerted by the bending die at the intrados as well as the significant tensile stress at the extrados as stated earlier. The oval-

ization in laser bending however is smaller than that in mechanical bending because no die is used and tensile stress at the extrados is greatly reduced.

#### 4 Experiment

As stated earlier, it is essential that the ratio of laser beam diameter,  $d$ , to tube thickness,  $t$  is high so that there is no steep temperature gradient in the direction of the wall thickness. The chosen ratio  $d/t$  ranges from 12.4 up to 16.9. The thickness of the tube is 0.89 mm and length 100 mm. The material of the tube is low carbon steel AISI 1010. To increase coupling of laser power, the samples were coated with graphite after cleaning using propanol. Absorption coefficient was obtained as described in Arnet and Vollertsen's paper [10]. During scanning, one end of the tube was clamped as shown in Fig. 1. Each tube was scanned ten times with still air cooling inbetween except one case indicated in the discussion section where forced air cooling was used. The CO<sub>2</sub> laser system used has the maximum power of 1.5 kW. The power density used is Gaussian distribution (Transverse Electromagnetic Mode (TEM)<sub>00</sub>). Laser beam diameter is defined as the diameter

**Table 1** The experimental and simulation conditions for laser forming of tubes

No.	Power (W)	Scanning speed (rad/s)	Beam diam. (mm)	Max scanning angle, $\theta_{max}$ (deg)	Ratio $D/t^*$
1	780	1.57-2.63	11	180	14.3
2	780, 1200	1.57, 2.63	11	180-322	14.3
3	500-780	1.57	11	180	14.3
4	780	1.57	11-15	270	14.3-28.5

\*  $D$  is the tube outer diameter and  $t$  the wall thickness

at which the power density becomes  $1/e^2$  of the maximum power value. The process parameters used in this work are shown in Table 1, which are also used in simulation.

The deformation of the tube including the bending angle, wall thickness change, extent of ovalization, and curvature were measured by a coordinate-measuring machine. To show the protrusion at the intrados a Scanning Electron Microscope (SEM) was used to image the axial sectioning of the bent tube.

## 5 Numerical Simulation

In the model of the finite element analysis (FEA), nonlinear analysis is used because of characteristics of the laser bending process of tubes. In the creation of mesh seed, a cluster function is used along the axial direction of the tube. Therefore, the width of area with a denser mesh is larger than that using one way bias. That is better for the tubing forming process associated with the large beam diameter. The same mesh is created for both thermal and structural analyses. In the FEA numerical simulation using code ABAQUS, three-dimensional heat-transfer elements with eight nodes DC3D8 and continuum stress/displacement elements with the same dimension and number of nodes C3D8 are used for the thermal and structural analyses respectively. A user-defined subroutine is developed using FORTRAN to define the magnitude of the heat flux generated by the laser beam for specific positions, which depends on the coupled laser power, beam diameter, scanning speed, and scanning scheme.

The following assumptions are made for the numerical modeling. Heat generated by plastic deformation is small compared with heat input by laser beam so that it can be neglected. A sequential thermal-mechanical analysis, therefore, is used in the simulation. Heating and deformation are symmetrical about the scanned plane and therefore only half tube is simulated. No melting occurs during the laser forming process. The tube under analysis is isotropic and work hardening material. The total deformation consists of the elastic strain, plastic strain, and thermal strain.

The boundary conditions used are as follows. No movement across the scanning plane (plane of symmetry) takes place during laser forming of the tubes. Surface free convection  $q = h(T - T^\circ)$ , where  $h = h(\mathbf{x}, t)$  is the film coefficient, and  $T^\circ = T^\circ(\mathbf{x}, t)$  the surrounding temperature, and radiation  $q = A((T - T^z)^4 - (T^\circ - T^z)^4)$ , where  $A$  is the radiation constant and  $T^z$  the absolute zero on the temperature scale used. The symmetric plane is under the adiabatic condition.

In numerical simulation, a general Hooke's law is used for elastic deformation and Von Mises criterion is used as the yield criterion. Plastic deformation of the workpiece follows the flow rule. In this simulation, the isotropic hardening rule and its yield locus are adopted. The relationship between the flow stress and strain is given by  $\sigma = C\varepsilon^n$ , where  $\sigma$  is the flow stress,  $\varepsilon$  the strain,  $n$  the work-hardening exponent,  $C$  is the strength coefficient. The influence of strain rate on flow stress is also taken into account [11]. Temperature dependent material properties, such as flow stress, thermal conductivity, specific heat, and Young's modulus, are also considered in the numerical simulation [12].

## 6 A Simple Closed-Form Expression of the Bending Angle

Although the necessity of FEM modeling has been recognized and planned as described above, a closed-form expression for the bending angle in a laser-bending process of tubes is derived. It is desirable to have closed-form solutions but only limited results can be obtained in many situations like in this case even after considerable simplifications are made. The closed-form expression depicts explicit dependence of the bending angle on process parameters and material properties.

In laser bending of tubes, the ratio between the laser beam diameter and wall thickness of the tube is kept high, and the scanning speed low in order to obtain a near homogeneous tem-

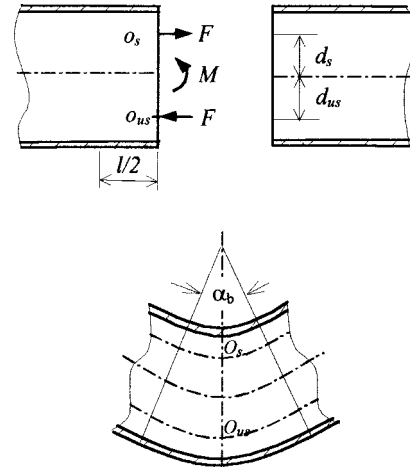


Fig. 2 Simplified model of laser bent tube

perature distribution through the wall thickness direction. Therefore, the temperature rise,  $\Delta T$ , on the outer and inner tube surfaces of the scanned region can be assumed to be identical. The elongation  $\Delta l_{th}$  in the axial direction of the tube caused by  $\Delta T$  can be written as

$$\Delta l_{th} = \alpha \Delta T l \quad (1)$$

where  $\alpha$  is the coefficient of thermal expansion,  $l$  the length of the heat affected zone in the axial direction (Fig. 2). As the flow stress in the heat-affected zone is greatly lowered by the temperature rise, and the surrounding unheated material severely constrains the expansion, the thermal expansion can be assumed to be converted into compressive plastic deformation [13].

Figure 2 shows the geometry of a tube before and after laser bending, and the forces and moment the tube is subjected to. It is assumed that only the top half of the tube is heated (that is, the maximum scanning angle,  $\theta_{max}$ , is 180 deg). The average strain of the scanned upper portion of the tube in the axial direction at the centroid  $O_s$  can be written as

$$\varepsilon_s = \frac{F}{a_s E_s} - \frac{M}{Z E_s} - \frac{\Delta T \alpha}{2} \quad (2)$$

where  $a_s$  is the area of upper portion of the tube,  $E_s$  the secant modulus,  $Z$  is the plastic modulus. Because the thermal induced strain in the axial direction is near zero at the beginning and end of the scanning, its average value that is  $\Delta T \alpha / 2$ , is used in the calculation. The strain of the unscanned portion in the axial direction can be written as

$$\varepsilon_{us} = -\frac{F}{a_s E_s} + \frac{M}{Z E_s} \quad (3)$$

$F$  and  $M$  are respectively

$$F = \Delta T \alpha a_s E_s / 2 \quad (4)$$

$$M = F(d_s + d_{us}) \quad (5)$$

where  $d_s$  is the distance from  $O_s$ , to the interface surface between scanned and unscanned portions and  $d_{us}$  is the distance from the  $O_{us}$ , the centroidal point of the scanned portion, to the interface surface between scanned and unscanned portions. The curvature is assumed to be constant along the curved region of the bent tube. The bending angle is caused by the strain difference between scanned and unscanned portions and can be written as

$$\alpha_b = \frac{l(\varepsilon_{us} - \varepsilon_s)}{d_s + d_{us}} \quad (6)$$

Combining Eqs. (2) to (6), one obtains

$$\alpha_b = \frac{l\Delta T\alpha}{2(d_s + d_{us})} \left( \frac{2a_s(d_s + d_{us})}{Z} - 1 \right) \quad (7)$$

$d_s$ ,  $d_{us}$  and  $Z$  can be written as

$$d_s = d_{us} = \frac{D}{\pi} \quad (8)$$

$$Z = D^2 t \quad (9)$$

$$a_s = \frac{\pi D t}{2} \quad (10)$$

where  $D$  is the diameter of the tube. Therefore, Eq. (7) reduces to

$$\alpha_b = \frac{0.78l\Delta T\alpha}{D} \quad (11)$$

The ratio  $\nu$  of the conductively dissipated power to laser input power has been written as [14]

$$\nu = \beta k^\mu \quad (12)$$

where  $k$  is the thermal conductivity, and  $\beta$  and  $\mu$  are functions of process parameters. Therefore, the heat energy generated by laser for the forming can be written as

$$E = t_s P \eta (1 - \beta k^\mu) \quad (13)$$

where  $P$  is the laser power,  $\eta$  the absorption coefficient of laser, and  $t_s$  the time period of laser scan and can be given as

$$t_s = \frac{2l_t}{D\omega} \quad (14)$$

where  $l_t$  is the length of the heat affected zone in the circumference direction and  $\omega$  the scanning speed of the laser beam. The following equation, therefore, holds

$$E = \Delta T l_t l \rho c_p \quad (15)$$

where  $t$  is the wall thickness of the tube,  $\rho$  the density,  $c_p$  the specific heat. Comparing Eqs. (13) and (15) leads to

$$\Delta T l = \frac{2P\eta(1 - \beta k^\mu)}{\omega D t \rho c_p} \quad (16)$$

Substituting Eq. (16) into Eq. (11) one obtains

$$\alpha_b = \frac{1.56\alpha P \eta (1 - \beta k^\mu)}{D^2 t \omega \rho c_p} \quad (17)$$

## 7 Results and Discussion

**7.1 Bending Angle.** Figures 3(a) and 3(b) compare the analytic, experimental and numerical results of the bending angle vs.

scanning speed and laser power, respectively. The simulation results agree with the experimental measurements, while the analytic solution displays a similar trend but different slope. The discrepancies between the analytic and experimental/simulation results are understood since simplifications were made in the derivation of the closed-form solution (Eq. (16)). To help analyze sources of the discrepancies, the value of  $\beta$  and  $\mu$  are adjusted such that the curves are approximately superposed at the lowest scanning speed in Fig. 3(a), and at highest laser power in Fig. 3(b). With increasing scanning speed, temperature in the heat affected zone decreases. With temperature decreasing, absorption coefficient decreases and thermal expansion coefficient and specific heat increase within the range of temperature examined. The increase in the specific heat, however, nearly doubles that in the thermal expansion coefficient. The combined effect of these changes is to make the calculated result, which does not take into account the temperature dependency of these properties, reduce slower than the experimental and simulation results (Fig. 3(a)). When the laser power increases, the temperature increases. Similar to the analysis above, the slope of the calculated results is not as steep as the experimental and simulation ones (Fig. 3(b)).

**7.2 Variation in the Wall Thickness.** The simulated shape of a laser formed tube is shown in Fig. 1(b) and compared with the undeformed one. Only half of the tube was simulated due to the symmetry of the deformation about the scanning plane. It can be seen that the material in the intrados moves outward in the radial direction and shortened in the longitudinal direction as indicated by the distorted mesh. The experimental and simulated change in wall thickness is shown in Fig. 4(a). As expected, the maximum thickening of less than 1 percent occurs at the intrados, while there is no appreciable thinning at the extrados. This is one of the major advantages of the laser bending process of tubes. To help understand the pattern of wall thickness variation, plastic strain in the axial and radial directions at the outer and inner surfaces are plotted in Fig. 4(b). As seen, the amount of axial compressive strain caused by thermal expansion is approximately matched by the radial tensile strain as required by the rule of volume constancy. Shown in Fig. 5 is a typical contour plot of the radial plastic strain in the scanning plane.

**7.3 Inner Surface of the Scanned Region.** Figure 6 presents the experimental measurement, numerical results and a photograph of the axial cross section of a laser-formed tube. It is interesting to note that the inner surface of the scanned region exhibits an outward bulge radially, which is counterintuitive, as the region was thickened during the bending process. This can be explained by the vertical component of the circumferential stress

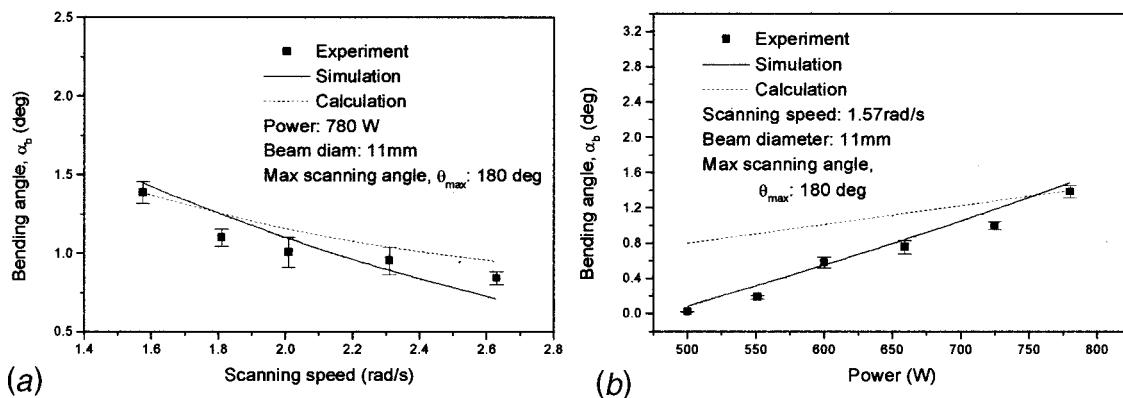


Fig. 3 Comparison of analytic, numerical, and experimental results of the bending angle vs. scanning speed (a) and laser power (b) (tube outer diameter: 12.7 mm, wall thickness: 0.89 mm).

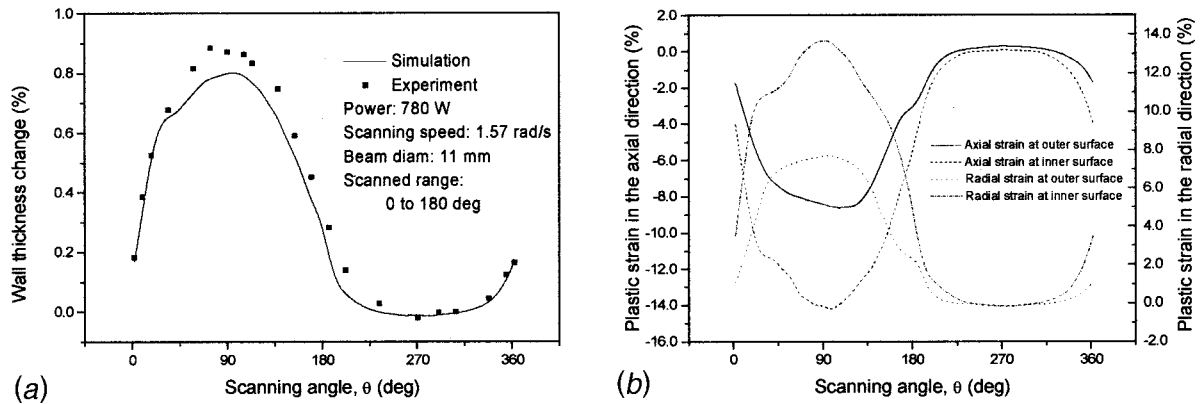


Fig. 4 (a) Variation of wall thickness and plastic strains in the radial and axial directions at the scanning plane (power: 780 W, scanning speed: 1.57 rad/s, beam diameter: 11 mm, max scanning angle: 180 degree, tube outer diameter: 12.7 mm, wall thickness: 0.89 mm)

indicated in Fig. 1(a), which also explains why the axial plastic strain at the outer surface is smaller than that at the inner surface (Fig. 4).

**7.4 Ovalization of the Cross Section.** Figure 7(a) shows numerical and experimental results of ovalization of the bent tube vs. laser power used. The ovalization is defined as  $(D_{\max} - D_{\min})/D$ , where  $D_{\max}$  and  $D_{\min}$  are the maximum and minimum deformed diameters, respectively, and  $D$  is the undeformed tube diameter. As seen from Fig. 7(b), at the beginning and end of laser scanning (about 1 deg and 180 deg), the outward displacement stated earlier is more intensive due to the stronger constraint from the surrounding material as compared to the middle region of the scanning (about 90 deg). At about 270 deg, the middle of the unscanned region, the radial displacement is about zero. Therefore, the elongation in the horizontal direction is greater than that in the vertical direction and an oval cross section is formed. With increasing laser power, the situation just mentioned becomes more pronounced and ovalization increases, although it remains much smaller than that seen in mechanical bending of tubes. In me-

chanical bending of tubes, the magnitude of ovalization can reach 20 percent for some bending processes without a mandrel [6].

**7.5 Asymmetry.** Figure 5 shows the formed tube is asymmetry about the vertical axis. This is further shown in a top view in Fig. 8(a). It can be seen that the bent tube slightly tilts rightwards because the temperature at the end of scanning is higher than that at the beginning as shown in Fig. 8(c). Higher temperature produces more deformation in the axial direction. As a result, the centerline of the bent tube shifts rightward as shown in Fig. 8(a). It can be seen from Figs. 8(a) and (b) that the diameter of the scanned area increases because of thickening of the materials near scanning.

To overcome the asymmetry, one may employ different process parameters or scanning schemes. One of the options is to scan using a varying angular speed. Increasing the scanning speed near the end of the scanning can reduce the temperature there. Figure 8(b) shows that the deformation becomes more symmetric. This is due to the more symmetric temperature along the circumferential direction affected by an empirically determined speed profile (Fig. 8(c)). Another approach examined in this work is to use a two-

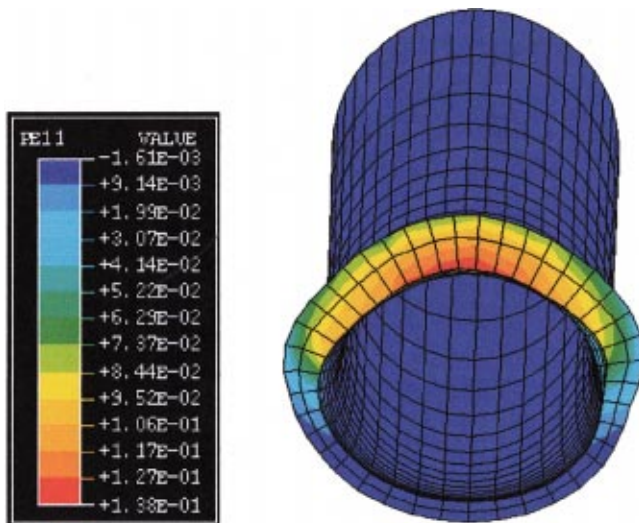


Fig. 5 Contour of plastic strain in the radial direction (half tube shown due to symmetry about the scanning plane, deformation magnification  $\times 15$ , power: 780 W, scanning speed: 1.57 rad/s, beam diameter: 11 mm, max scanning angle: 180 degree, tube outer diameter: 12.7 mm, wall thickness: 0.89 mm)

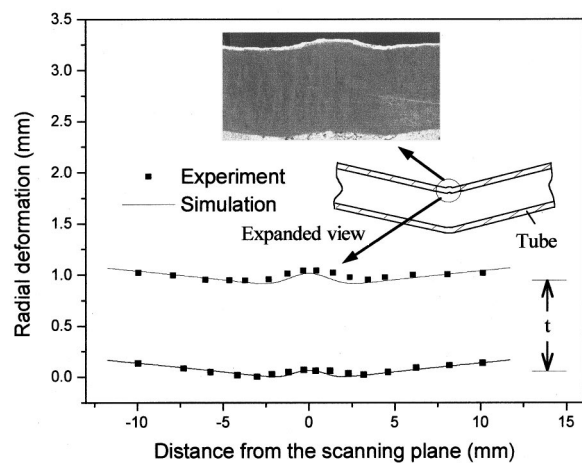


Fig. 6 Simulation and experimental measurements of the protruded intrados at the axial cross section ( $t$ : original wall thickness) and photograph of the protruded intrados (vertical/horizontal magnification=5:1) (power: 780 W, scanning speed: 1.57 rad/s, beam diameter: 11 mm, maximum scanning angle,  $\theta_{\max}$ : 180 degree, tube outer diameter: 12.7 mm, wall thickness: 0.89 mm)

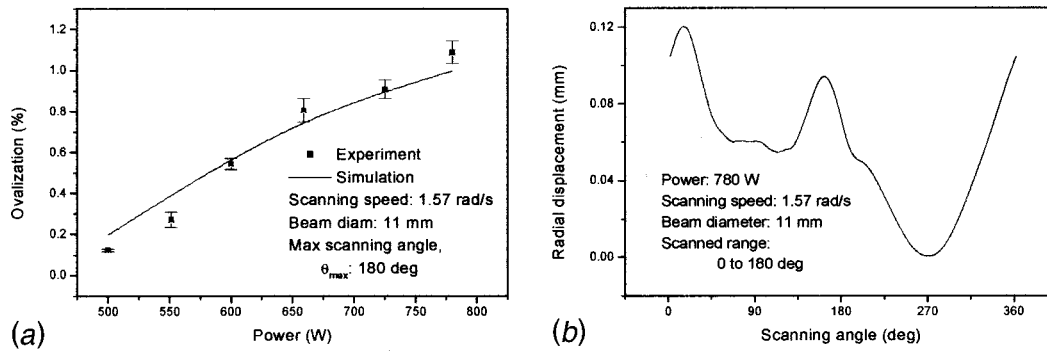


Fig. 7 (a) Simulation and experimental results of ovalization of the cross section at the scanning plane (b) Simulation results of the radial displacements of the outer surface at the scanning plane (tube outer diameter: 12.7 mm, wall thickness: 0.89 mm)

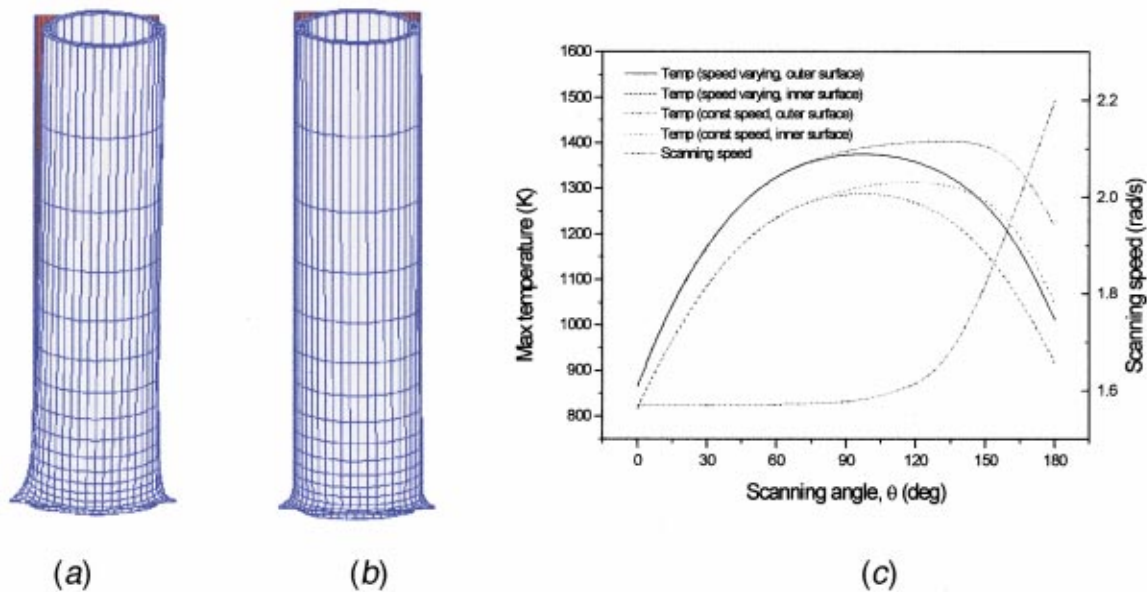


Fig. 8 (a) Asymmetry of deformation, i.e., tilting rightwards as seen from this top view (half tube shown due to symmetry about the scanning plane, magnification  $\times 20$ ) (b) Improvement of symmetry by varying the scanning speed ( $\times 20$ ), and (c) Variation of maximum temperature under the conditions of the constant scanning speed (1.57 rad/s) and the varying scanning speed (power: 780 W, beam diameter: 11 mm, max scanning angle,  $\theta_{max}$ : 180 deg, tube outer diameter: 12.7 mm, wall thickness: 0.89 mm)

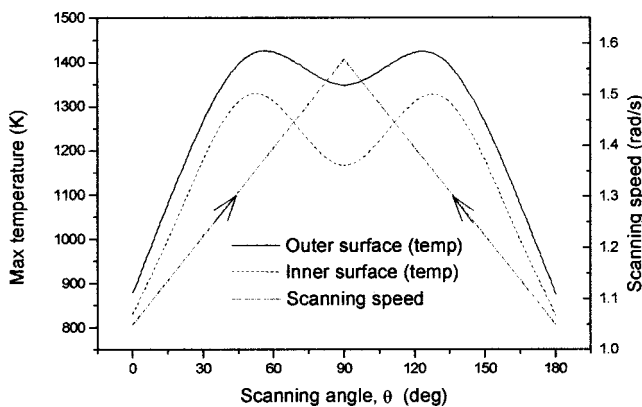


Fig. 9 Variation of maximum temperature under the two-segment scanning scheme (0 deg to 90 deg and then 180 deg to 90 deg) (power: 780 W, beam diameter: 11 mm, max scanning angle,  $\theta_{max}$ : 180 deg, tube outer diameter: 12.7 mm, wall thickness: 0.89 mm)

segment scanning scheme, that is, first scanning from 0 to 90 degrees, and then from 180 to 90 degrees (Fig. 9). The variation of the maximum temperature obtained from this scheme is also shown in Fig. 9. As seen, temperature is more symmetric about the vertical axis, and as a result, the deformed shape is more symmetric, similar to the case shown in Fig. 8(b).

**7.6 Effect of the Maximum Scanning Angle.** So far, only bending results under  $\theta_{max}=180$  deg have been presented. The effect of maximum scanning angle,  $\theta_{max}$  on the bending angle is shown in Fig. 10(a). Under the conditions examined, the bending angle increases with  $\theta_{max}$  to a maximum value, before it drops. As a tube is laser bent, the material in the scanned region is shortened and the material of the unscanned region is bent by the moment caused by the shortening. With  $\theta_{max}$  increasing, the unscanned region reduces. This makes the resistance against bending of this region lower so that the bending angle rises. When  $\theta_{max}$  further increases, the tube tends to be scanned along its entire circumference and as a result, the bending efficiency drops.

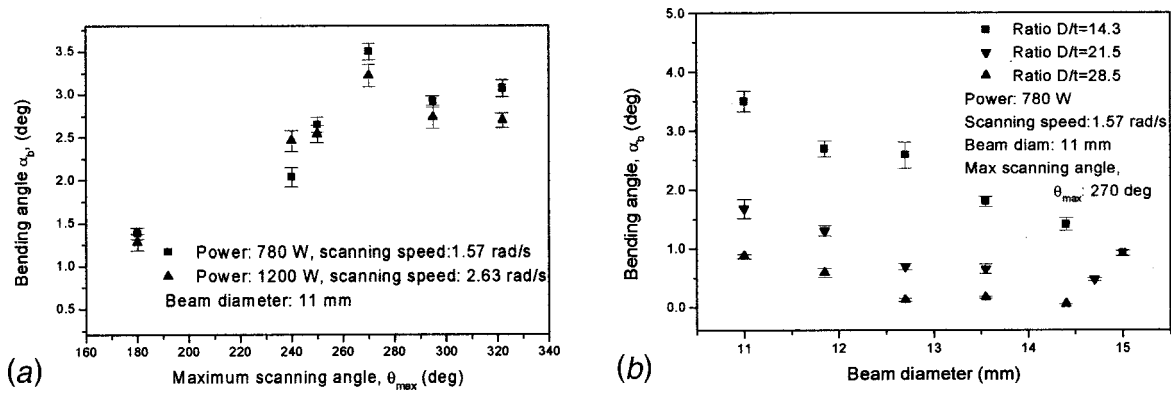


Fig. 10 (a) Variation of the bending angle with the max scanning angle (tube outer diameter: 12.7 mm, wall thickness: 0.89 mm) and (b) Dependence of the bending angle on the beam diameter for different ratios of tube outer diameter,  $D$ , to wall thickness,  $t$  ( $t=0.89$  mm).

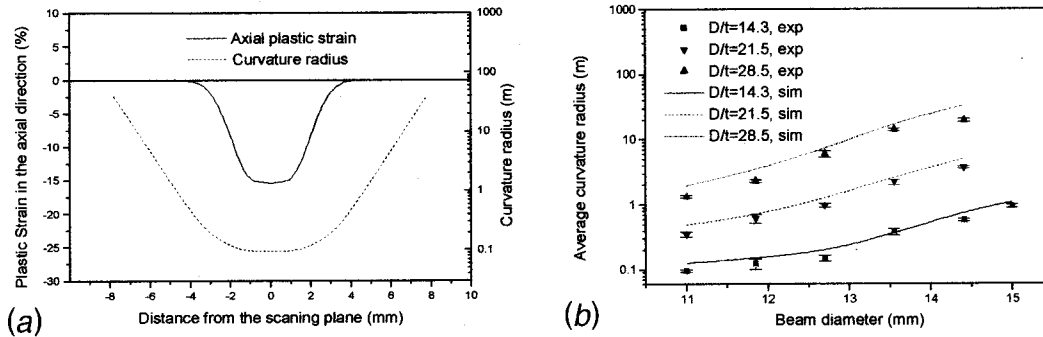


Fig. 11 (a) Axial plastic strain on the outer surface at the intrados and curvature radius vs. distance from the scanning plane (b) Average curvature radius of the bent tube vs. beam diameter for different ratios of outer diameter vs. wall thickness (power: 780 W, scanning speed: 1.57 rad/s, maximum scanning angle: 270 degree, wall thickness: 0.89 mm)

**7.7 Beam Diameter, Tube Size, and Minimum Bending Radius.** The influence of the laser beam diameter on the bending angle is presented in Fig. 10(b) for different ratios of the tube outer diameter,  $D$ , to the wall thickness,  $t$ . The bending angle decreases with increasing beam diameter because of the reduced laser intensity. The bending angle also decreases with increasing ratio  $D/t$ . As the ratio increases, the distance between the scanned and unscanned regions increases but the shortening of the scanned region remains approximately unchanged. As a result, the bending angle decreases.

Shown in Fig. 11(a) are the axial plastic strain at the intrados and the curvature radius vs. the distance from the scanning plane. The curvature radius is the radius of curvature of the centerline of a bent tube after scanning. As seen, the compressive plastic strain occurs only over a short distance of about 7 to 8 mm (less than the beam diameter of 11 mm and note the laser beam diameter is defined as the diameter at which the power density becomes  $1/e^2$  of the maximum power at the beam center). It is also seen that the curvature radius over this distance changes moderately. Based on the observation, it is reasonable to use a single curvature radius averaged over this distance (Figs. 2 and 11(b)). In mechanical bending, the deformation region is normally much larger and the curvature radius varies over the region.

Figure 11(b) shows the dependence of the average curvature radius on the laser beam diameter. As seen, the curvature radius increases with the beam diameter. This is because the dimension of the deformed area in the axial direction increases and thus the arc length of the curved region. At the same time, the bending angle decreases due to reduced energy intensity (Fig. 10(b)). Both result in rise of the curvature radius. It can also be seen from Fig. 11(b) that the curvature radius increases with the outer diameter/

thickness ratio,  $D/t$ . With increasing ratio, the bending angle decreases while the arc length of the curved region remain more or less unchanged. As a result, the curvature radius increases.

For conventional mechanical bending, the minimum bending radius is mainly governed by the elongation of the material at the extrados and the tube outer diameter. For laser bending of tubes, there is little elongation at the extrados and therefore the elongation is not a determining factor of the minimal bending radius. As

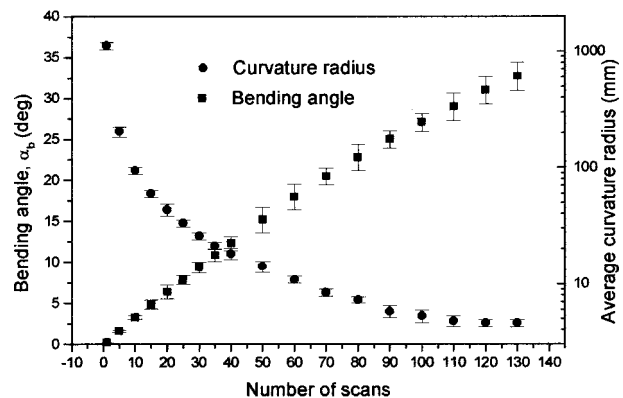


Fig. 12 Experimental results of the bending angle and average curvature radius vs. number of scans (power: 780 W, scanning speed: 1.57 rad/s, beam diameter: 11 mm, maximum scanning angle: 270 degree, tube outer diameter: 12.7 mm, wall thickness: 0.89 mm)

seen from Fig. 11(b), the smaller the beam size, the smaller the average curvature radius. But the upsetting mechanism of laser bending of tubes requires the beam diameter at least ten times of the tube thickness. At the same time, the smaller the outer diameter/thickness ratio is, the smaller the average curvature radius.

For given tube and beam diameter, the average curvature radius also decreases with increase of the bending angle (Fig. 12) for the reason already stated earlier. But the increase and the decrease in particular slow down as the tube is being further bent due to work-hardening effect. Therefore it is reasonable to conclude that the minimal bending radius in laser forming of tubes depends on laser beam size, tube thickness and outer diameter, and material properties such as work-hardening.

## 8 Conclusions

The mechanisms of laser bending of tubes are a combination of thickening of the laser-scanned region due to thermally induced axial compressive stress, and a slightly outward displacement of the region caused by a component of the thermally induced circumferential compressive stress. As a result, bending is primarily achieved through the thickening of the scanned region instead of the thinning of the unscanned region, and the scanned region assumes a slightly protruded shape. The absence of appreciable wall thinning is one of the major advantages of laser bent tubes. Cross-section ovalization of the laser-bent tubes is also much smaller than that observed in comparable mechanical bent tubes due to lack of bending die and appreciable tensile stress/strain in the extrados. The bending radius is governed by the laser beam diameter, not by tensile failure at the extrados. The curvature radii of the bent tube increase with the beam diameter and the ratio of the tube outer diameter to the wall thickness. The bending efficiency increases with the maximum scanning angle up to a critical value.

Asymmetry of the bending process can be reduced by varying the scanning speed or employing a two-segment scanning scheme.

## References

- [1] Kervick, R. J., and Springborn, R. K., 1966, "Cold Bending and Forming Tube and Other Section," ASTME, Michigan.
- [2] Karman, Th. V., 1911, "Über die Formänderung Dünnwandiger Rohre, Insbesondere Federnder Ausgleichsrohre," *Z. Ver. Deit. Ing.*, **55**, pp. 1889–1895.
- [3] Brazier, L. G., 1927, "On Flexure of Thin Cylindrical Shell and Other Thin Sections," *Proc. R. Soc. London, Ser. A*, **116**, pp. 104–14.
- [4] Zhang, L. C., and Yu, T. X., 1987, "An Investigation of the Brazier Effect of a Cylindrical Tube Under Pure Elastic-Plastic Bending," *Int. J. Pressure Vessels Piping*, **30**, pp. 77–86.
- [5] Wierzbicki, T., and Sinmal, M. V., 1997, "A Simplified Model of Brazier Effect in Plastic Bending of Cylindrical Tubes," *Int. J. Pressure Vessels Piping*, **71**, pp. 19–28.
- [6] Pan, K., and Stelson, K. A., 1995, "On the Plastic Deformation of a Tube During Bending," *ASME J. Ind.*, **117**, pp. 494–500.
- [7] Silve, S., Steen, W. M., and Podschies, B., 1998, "Laser Forming Tubes: A Discussion of Principles," *Proceedings of ICALEO*, Section E, pp. 151–160.
- [8] Frackiewicz, H., Trampczynski, W., and Przetakiewicz, W., 1992, "Shaping of Tubes by Laser Beam," *Proceedings of the 25th International Symposium on Automotive Technology and Automation*, ISATA 25th, pp. 373–380.
- [9] Kraus, J., 1997, "Basic Process in Laser Bending of Extrusion Using the Upsetting Mechanism," *Laser Assisted Net shape Engineering 2, Proceedings of the LANE'97*, Meisenbach Bamberg, Germany, Vol. 2, pp. 431–438.
- [10] Arnet, H., and Vollertsen, F., 1995, "Extending Laser Bending for the Generation of Convex Shapes," *IMEchE Part B: Journal of Engineering Manufacture*, **209**, pp. 433–442.
- [11] Li, W., and Yao, Y. L., 1999, "Numerical and Experimental Study of Strain Rate Effects in Laser Forming," *ASME J. Manuf. Sci. Eng.*, **122**, No. 3, 2000, pp. 445–451.
- [12] Li, W., and Yao, Y. L., 1999, "Convex Laser Forming with High Certainty," *Proc. The North American Manufacturing Research Conference XXVIII*, Lexington, KY, May, 2000, pp. 33–38.
- [13] Vollertsen, F., 1994, "An Analytical Model for Laser Bending," *Lasers Eng.*, **2**, pp. 261–276.
- [14] Schulz, W., Becker, D., Franke, J., Kemmerling, R., and Herziger, G., 1993, "Heat Conduction Losses in Laser Cutting of Metals," *J. Phys. D*, **26**, pp. 1357–1363.